Scanning tunneling microscopy for imaging and quantification of defects in as-deposited MoS_2 monolayers on sapphire substrates

Y. Rybalchenko[a,b,*], A. Minj[a], H. Medina[a], R. Villarreal[c], B. Groven[a], D. Lin[a], L. M. C. Pereira[c], P. Morin[a], T. Hantschel[a], V. V. Afanas'ev[a,b]

[a] *IMEC, Kapeldreef 75, Leuven, 3001, Belgium*
[b] *KU Leuven, Semiconductor Physics, Celestijnenlaan 200d, Leuven, 3001, Belgium*
[c] *KU Leuven, Quantum Solid State Physics, Celestijnenlaan 200d, Leuven, 3001, Belgium*

Abstract

This paper quantitatively assessed the intrinsic defectivity of as-deposited molybdenum disulfide (MoS_2) monolayers on sapphire substrates using atomically resolved scanning tunneling microscopy and spectroscopy. We observed two types of point defects – protrusion-like and depression-like with average densities of $(2.4\pm2)\cdot10^{13}$ cm^{-2} and $(1.9\pm1.4)\cdot10^{12}$ cm^{-2}, respectively. The position of the electron state within the MoS_2 bandgap suggests that the protrusion-like defect associates with a sulfur mono-vacancy.

Keywords: scanning tunneling microscopy, 2D semiconductors, synthetic molybdenum disulfide, point defects, sapphire substrate

1. Introduction

Synthetic two-dimensional transition metal dichalcogenides (TMDs) promise a viable solution to continue nanoelectronic device downscaling beyond 2 nm technology nodes where the Si-based transistors get penalized by short-channel effects [1]. Among TMDs, molybdenum disulfide (MoS_2) monolayer (ML) channels have demonstrated the highest mobilities so far [2]. However, electron mobilities in synthetic MoS_2 channels are still far below the theoretically predicted values [3]. The presence of inter- and intra-grain defects in these layers is suspected as the major factor responsible for the degradation of electronic properties of synthetic TMD channels [4, 5]. To minimize the number of grain boundaries, a single crystalline c-plane sapphire substrate has been used as a template for epitaxial growth of MoS_2 ML [2]. To further optimize the MoS_2 deposition process – one needs to identify and quantify intrinsic defects on pristine as-deposited layers and understand their dependence on the growth conditions.

Transmission electron microscopy has been routinely used to identify and quantify point and extended defects on MoS_2 [6]. However, the high energy of electron beams can cause additional damage [6], while the mandatory water-assisted transfer of the film onto a metallic grid can introduce additional Mo vacancy related defects [7]. Scanning tunneling microscopy (STM) is more suitable to study the as-deposited layers as it does not require potentially damaging sample preparation steps. STM has been extensively used to analyze synthetic TMD films grown on conductive substrates [8]; however, it encounters difficulties when analyzing layers grown on insulating substrates such as c-plane sapphire. Here, we demonstrate the first successful use of STM to directly observe and quantify point defects in as-deposited MoS_2 ML on sapphire substrates.

2. Methods

MoS_2 MLs were deposited at 1000 ºC using a commercial 2-inch (~50 mm) c-plane 1º off-axis cut sapphire substrate using metal organic chemical vapor deposition from $Mo(CO)_6$ and H_2S precursors carried by Ar and N_2 gas flows, respectively [9]. Then, the wafers were transported inside an Ar-filled glove box, where they were cleaved into 0.6×0.6 cm^2 samples. STM topographic images were obtained using a positive sample bias (probing unoccupied states) in the constant current mode. Two types of STM characterizations were performed – a large-scale (scan size up to 100 by 100 nm^2) and a high-resolution (up to 20 by 20 nm^2). A fast-drying silver paint and a 0.05 mm thick tantalum foil were used to realize the side electrical contacts to MoS_2 MLs for former and latter one, respectively. Fig. 1A shows the schematics of our STM setup. Large-scale STM topographic images were taken 1 month after the growth using a Park NX Hivac atomic force microscopy system in high vacuum (10^{-5} Torr). High-resolution STM topographic images were obtained 7 months after growth using an Omicron low-temperature STM system in ultra-high vacuum ($3\cdot10^{-12}$ Torr) at 77.5 K. Differential conductance (dI/dV) images were obtained simultaneously with topography by lock-in detection of the alternating current induced by a modulation voltage (20 mV) at a frequency of 890 Hz with an integration time of 1 ms. Scanning tunneling spectroscopy (STS) was performed using the same parameters as for the dI/dV images but with an increased integration time of 10 ms. High-resolution images were collected on the sample before and after vacuum annealing at 165 ºC for 7 days intended to remove adsorbates. In total, the MoS_2 samples got exposed to the atmosphere for about 30 minutes dur-

*Corresponding author at IMEC, Kapeldreef 75, Leuven, 3001, Belgium
Email address: yevhenii.rybalchencko@imec.be (Y. Rybalchenko)

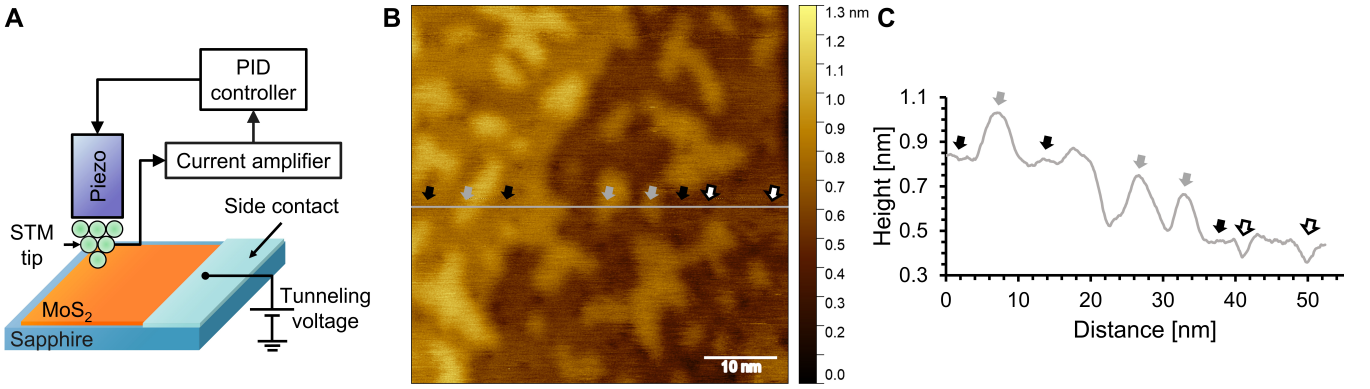

Figure 1: (A) Schematic of STM measurement setup. (B) Large-scale STM image of as-deposited MoS_2 ML on sapphire (V_{sam} = 1 V, I_s = 0.4 nA) and (C) height profile of the line in (B) showcasing all major topographical features with arrows: MoS_2 ML on sapphire terrace (black), water intercalated area (gray) and defect-related pits (white).

ing transport. Between growth and measurements, the samples were stored in a load lock of a glove box with the pressure kept at $7.5{\cdot}10^{-2}$ Torr.

3. Results and Discussion

The large-scale STM images reveal three distinctive topographical features of the MoS_2 ML surface (Fig. 1B). The first one is a fully closed and continuous MoS_2 ML on the sapphire substrate with its distinct step and terrace structure (indicated with black arrows). The second consists of areas with water intercalated between MoS_2 and sapphire (gray arrows) that most likely appear during a brief air exposure while transporting the sample to and from the glove box. The chemical nature of intercalated species was confirmed by Serron et al. using time-of-flight secondary ion mass spectrometry [10]. The third feature consists of pits (white arrows) occurring with an areal density of $(1.4{\pm}0.5){\cdot}10^{12}$ cm^{-2}.

Most pits are 0.1 to 0.3 nm deep and exhibit a circular shape with a diameter between 1 and 3 nm (Fig. 1C). However, their sizes can vary depending on the experimental conditions such as sample bias (V_{sam}) and current setpoint (I_s). The STM topography is a convolution of the surface structure and the local density of electron states (LDOS). Thus, the pit contrast arises due to the absence of unoccupied states (which were probed with the positive V_{sam}) at the defect site across the monolayer, and not from the actual "hole" in the MoS_2 surface. Observing point defects when the hexagonal lattice of MoS_2 is not resolved also agrees with the literature [11]. Bigger pits could suggest the presence of unresolved defect clusters.

The high-resolution STM images reveal that point defects indeed cause the pit contrast (Fig. 2). We observed two types of point defects (Fig. 3A): protrusion-like (indicated with white arrows) and depression-like (black arrows). The main visual difference between these two is that the former exhibits a hexagonal ring with a protrusion at its center while the latter is characterized by a single point like depression. However, since not all protrusion-like defects are surrounded by hexagonal rings, one might argue that those are different types of defects. dI/dV images that were obtained simultaneously with the topography im-

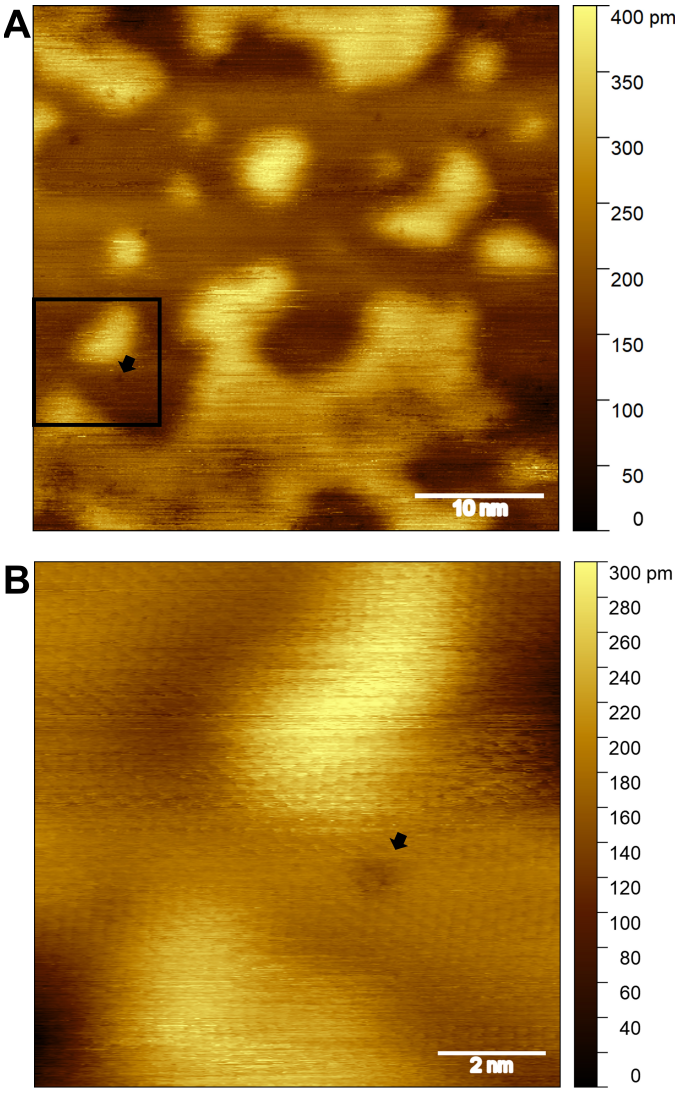

Figure 2: (A) Large-scale and (B) high-resolution STM images of MoS_2 ML on sapphire (V_{sam} = 1 V, I_s = 0.1 nA). (B) is a zoomed in image of the area in a black square on (A). Arrows indicate that pit on (A) corresponds to a point defect on (B).

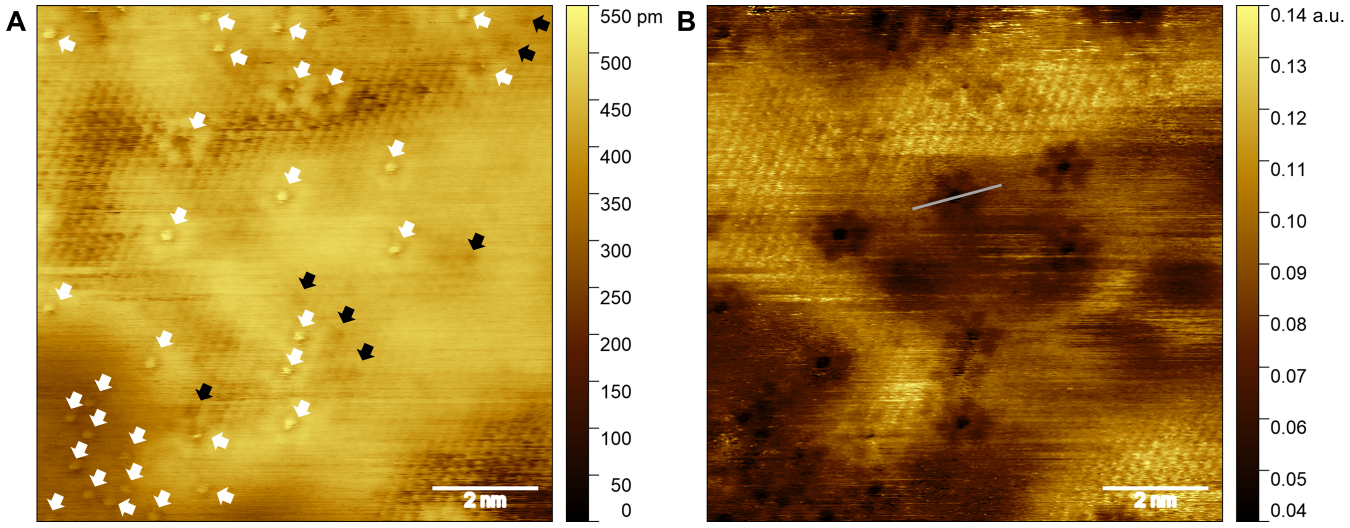

Figure 3: High-resolution STM images of as-deposited MoS_2 ML on a sapphire substrate (V_{sam} = 0.5 V, I_s = 0.2 nA). (A) Topography of MoS_2 ML showing 2 types of point defects – protrusion-like (white arrows) and depression-like (black arrows). (B) dI/dV image obtained simultaneously with (A) shows that all protrusion-like defects have a hexagonal ring around them.The abbreviation "a.u." stands for arbitrary units.

ages (Fig. 3B) reveal that all protrusions do possess an hexagonal ring around them which is not always resolved in the topography image. Depression-like defects, on the other hand, do not appear in the dI/dV image. As the dI/dV signal is proportional to the LDOS at the V_{sam}, the lack of contrast in the dI/dV images simply means that the LDOS of depression-like defects is the same as for the MoS_2 basal plane at this V_{sam}.

These two types of defects occur with different densities – $(2.4\pm2)\cdot10^{13}$ protrusion-like defects and $(1.9\pm1.4)\cdot10^{12}$ depression-like defects per cm^2. The error bar represents an average deviation across ~2000 nm^2 area. The estimated densities are comparable with those previously reported for synthetic layers, which range from 10^{12} [8] to 10^{13} cm^{-2} [11]. The defect distribution across the sample was non-uniform with the lowest total density of $2\cdot10^{12}$ cm^{-2} and the highest of $8.1\cdot10^{13}$ cm^{-2}. Similar lateral inhomogeneities were encountered in both exfoliated and synthetic MoS_2 [5, 11]. The low defect density observed on several locations promises the possibility of further growth process' optimizations towards less defective synthetic layers supported and enabled by the STM defect imaging and characterization.

To reveal the nature of the detected defects, we performed STS measurements in a 32 by 32 grid on a 10 by 10 nm^2 area near the location of Fig. 3A. Unfortunately, the topography image obtained right before the spectroscopy measurements does not have atomic resolution (Fig. 4A). However, there are depressions in the dI/dV image (Fig. 4B). Their lateral dimensions correspond to dI/dV imprint of topographical protrusion-like defects observed prior with atomic resolution at the same experimental conditions (Fig. 4C). This suggests the presence of these defects on the analyzed area. Two spectral features were most prominent (Fig. 4D, E) – the ~2 eV MoS_2 bandgap and an electron gap state at ~0.5 eV below the MoS_2 conduction band. These appeared in ~30% and ~50% out of the 1024 spectra, respectively. The remaining spectra were not conclusive. The observed electron gap state could point towards a sulfur mono-vacancy (V_S) as its origin [6]. The occurrence of the electron state on more than 50% of the obtained spectra indicates that a large portion of the studied area is covered with a single type of defect. This might suggest that the observed electron state stems from the protrusion-like defects as their density is 10 times higher than that of the depression-like defects. This would be consistent with the literature which predicts V_S to be the most abundant defect type due to its lowest formation energy [6]. Moreover, calculations based on the density functional theory (DFT) predict a protrusion surrounded by a hexagonal ring to be an STM image of a bottom sulfur mono-vacancy in a free-standing MoS_2 ML [11].

We cannot claim that the depression-like defects were present on the area in which STS was performed as they do not have a dI/dV imprint at this V_{sam}. However, based on DFT calculations by Zhou et al., the sulfur di-vacancy and the molybdenum vacancy should have the second lowest formation energy at different MoS_2 growth conditions [6] making them the most likely candidates to be associated with the depression-like defects. The former would also coincide with obtained STS data as the sulfur di-vacancy should have an electron gap state near the energy level of the V_S electron gap state [6].

Finally, we want to underline the drastic difference in the defect areal density estimated from the large-scale and atomically resolved STM images: $1.4\cdot10^{12}$ cm^{-2} for the former versus $2.6\cdot10^{13}$ cm^{-2} for the latter. This effect could be attributed to a higher resolution enabling the detection of point defects located close to each other. To confirm that the difference is not caused by the ageing of the sample, additional large-scale STM images were obtained 10 months after the growth. They show that the pit density remains unchanged: $(1.5\pm0.3)\cdot10^{12}$ cm^{-2}. Thus, atomic resolution is required for a reliable quantification of point defects in MoS_2 MLs.

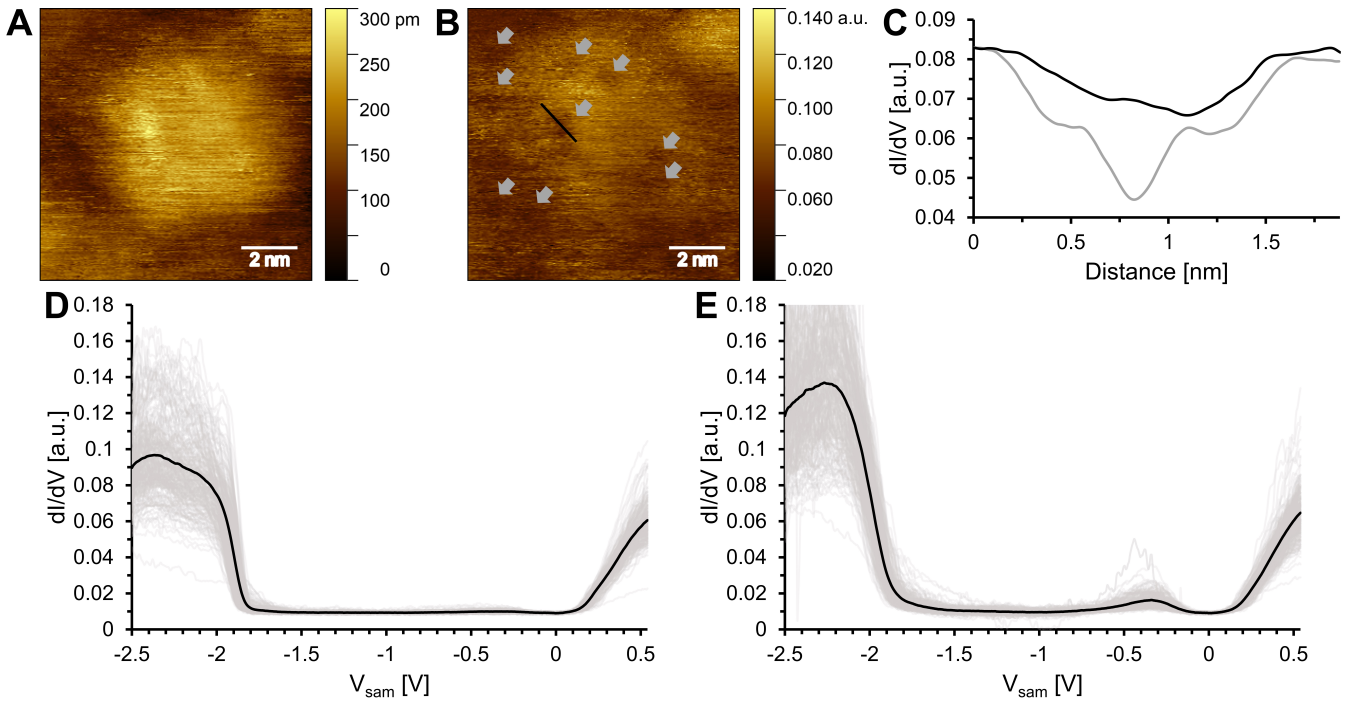

Figure 4: (A) Topography and (B) dI/dV images (V_{sam} = 0.5 V, I_s = 0.2 nA) of the location where STS spectra were obtained in a 32 by 32 grid. Gray arrows point towards depressions in dI/dV image that could correspond to topographical protrusion-like defects. (C) dI/dV profiles of lines across topographical protrusion-like defect in high-resolution STM from Fig. 3B (gray line) and dI/dV depression in Fig. 4B (black line). The most prominent spectral features from STS measurement – (D) ~2 eV MoS_2 bandgap and (E) an electron state at ~0.5 eV below conduction band. Black lines here represent an average dI/dV value of obtained spectra (gray lines) for each V_{sam}.

4. Conclusions

We succeeded in atomic STM characterization of point defects in an as-deposited synthetic MoS_2 ML on an insulating sapphire substrate. Two types of defects were distinguished – protrusion-like and depression-like with densities of $2.4{\cdot}10^{13}$ cm^{-2} and $1.9{\cdot}10^{12}$ cm^{-2}, respectively. The protrusion-like defect was provisionally identified as a sulfur mono-vacancy. Despite the possibility to observe the defects on the large-scale STM images, atomic resolution is a pre-requisite for the reliable quantification of defects in MoS_2 MLs. Our findings open the possibility to study the relationship between intrinsic defect formation in MoS_2 ML and the growth conditions aiming to reduce the intra-grain defectivity introduced by deposition process.

5. Acknowledgements

This work was done in the imec IIAP core CMOS programs and received funding from the European Union's Graphene Flagship grant agreement No 952792, 2D-experimental pilot line. It was also supported by the Research Foundation - Flanders (FWO) grant 1SG1123N, and by the FLAG-ERA grant DIMAG.

References

[1] IRDS™2022: Beyond CMOS and Emerging Materials Integration - IEEE IRDS™, https://irds.ieee.org/editions/2022/irds%E2%84%A2-2022-beyond-cmos-and-emerging-research-materials, accessed April 14, 2023 (2022).

[2] T. Li, W. Guo, L. Ma, W. Li, Z. Yu, Z. Han, S. Gao, L. Liu, D. Fan, Z. Wang, et al., Epitaxial growth of wafer-scale molybdenum disulfide semiconductor single crystals on sapphire, Nature Nanotechnology 16 (11) (2021) 1201–1207. doi:10.1038/s41565-021-00963-8.

[3] A. Afzalian, Ab initio perspective of ultra-scaled CMOS from 2D-material fundamentals to dynamically doped transistors, npj 2D Materials and Applications 5 (1) (2021) 5. doi:10.1038/s41699-020-00181-1.

[4] T. H. Ly, D. J. Perello, J. Zhao, Q. Deng, H. Kim, G. H. Han, S. H. Chae, H. Y. Jeong, Y. H. Lee, Misorientation-angle-dependent electrical transport across molybdenum disulfide grain boundaries, Nature communications 7 (1) (2016) 10426. doi:10.1038/ncomms10426.

[5] F.-X. R. Chen, N. Kawakami, C.-T. Lee, P.-Y. Shih, Z.-C. Wu, Y.-C. Yang, H.-W. Tu, W.-B. Jian, C. Hu, C.-L. Lin, Visualizing correlation between carrier mobility and defect density in MoS_2 FET, Applied Physics Letters 121 (15) (2022) 151601. doi:10.1063/5.0107938.

[6] W. Zhou, X. Zou, S. Najmaei, Z. Liu, Y. Shi, J. Kong, J. Lou, P. M. Ajayan, B. I. Yakobson, J.-C. Idrobo, Intrinsic structural defects in monolayer molybdenum disulfide, Nano letters 13 (6) (2013) 2615–2622. doi:10.1021/nl4007479.

[7] B. Schoenaers, A. Leonhardt, A. Mehta, A. Stesmans, D. Chiappe, I. Asselberghs, I. Radu, C. Huyghebaert, S. De Gendt, M. Houssa, et al., Analysis of transferred MoS_2 layers grown by MOCVD: evidence of Mo vacancy related defect formation, ECS Journal of Solid State Science and Technology 9 (9) (2020) 093001. doi:10.1149/2162-8777/ab8363.

[8] X. Liu, I. Balla, H. Bergeron, M. C. Hersam, Point defects and grain boundaries in rotationally commensurate MoS_2 on epitaxial graphene, The Journal of Physical Chemistry C 120 (37) (2016) 20798–20805. doi:10.1021/acs.jpcc.6b02073.

[9] Y. Shi, B. Groven, J. Serron, X. Wu, A. Nalin Mehta, A. Minj, S. Sergeant, H. Han, I. Asselberghs, D. Lin, et al., Engineering wafer-scale epitaxial two-dimensional materials through sapphire template screening for advanced high-performance nanoelectronics, ACS nano 15 (6) (2021) 9482–9494. doi:10.1021/acsnano.0c07761.

[10] J. Serron, A. Minj, V. Spampinato, A. Franquet, Y. Rybalchenko, M.-E.

Boulon, S. Brems, H. M. Silva, Y. Shi, B. Groven, et al., Conductivity enhancement in transition metal dichalcogenides: A complex water intercalation and desorption mechanism, ACS Applied Materials & Interfaces (2023). doi:10.1021/acsami.3c03057.

[11] I. D. Marion, D. Čapeta, B. Pielić, F. Faraguna, A. Gallardo, P. Pou, B. Biel, N. Vujičić, M. Kralj, Atomic-scale defects and electronic properties of a transferred synthesized MoS_2 monolayer, Nanotechnology 29 (30) (2018) 305703. doi:10.1088/1361-6528/aac27d.